Title

Global Rebalancing of Cellular Resources by Pleiotropic Point Mutations Illustrates a Multi-scale Mechanism of Adaptive Evolution

Journal

Cell Systems, 2(4)

ISSN

2405-4712

Authors

Utrilla, Jose
O'Brien, Edward J
Chen, Ke
et al.

Publication Date

2016-04-01

DOI

10.1016/j.cels.2016.04.003

Peer reviewed

HHS Public Access

Author manuscript

Cell Syst. Author manuscript; available in PMC 2017 April 27.

Published in final edited form as:

Cell Syst. 2016 April 27; 2(4): 260–271. doi:10.1016/j.cels.2016.04.003.

Global Rebalancing of Cellular Resources by Pleiotropic Point Mutations Illustrates a Multi-scale Mechanism of Adaptive Evolution

Jose Utrilla[1,2,†], **Edward J. O'Brien**[1,3,†], **Ke Chen**[1], **Douglas McCloskey**[1], **Jacky Cheung**[4], **Harris Wang**[4], **Dagoberto Armenta-Medina**[5], **Adam M. Feist**[1,6], and **Bernhard O. Palsson**[1,6,7,*]

[1]Department of Bioengineering, University of California San Diego, La Jolla, CA, USA

[2]Centro de Ciencias Genómicas. Universidad Nacional Autónoma de México. Cuernavaca, Morelos, México

[3]Bioinformatics and Systems Biology program, University of California, San Diego, La Jolla, CA, USA

[4]Department of Systems Biology, Columbia University, New York, NY, USA

[5]Departamento de Ingeniería Celular y Biocatálisis. Instituto de Biotecnología, UNAM. Cuernavaca, Morelos Mexico

[6]Novo Nordisk Foundation Center for Biosustainability, Technical University of Denmark, 2800 Lyngby, Denmark

[7]Department of Pediatrics, University of California, San Diego, CA 92093, USA

Summary

Pleiotropic regulatory mutations affect diverse cellular processes, posing a challenge to our understanding of genotype-phenotype relationships across multiple biological scales. Adaptive Laboratory Evolution (ALE) allows for such mutations to be found and characterized in the context of clear selection pressures. Here, several ALE-selected single-mutation variants in *Escherichia coli*'s RNA polymerase (RNAP) are detailed using an integrated multi-scale experimental and computational approach. While these mutations increase cellular growth rates in steady environments, they reduce tolerance to stress and environmental fluctuations. We detail structural changes in the RNAP that rewire the transcriptional machinery to rebalance proteome and energy allocation towards growth and away from several hedging and stress functions. We find

*Correspondence to: Bernhard O. Palsson palsson@eng.ucsd.edu.
†These authors contributed equally to this work

Author contributions: JU and BOP conceived the study. JU performed the physiological and RNA-seq experiments. DM performed metabolomics experiments. JC and HW generated mutation variants by MAGE. JU and EJO performed data processing and computational analysis. KC and DAM performed structural analysis. BOP supervised the study. AMF provided critical feedback. JU, EJO, KC and BOP wrote the manuscript

that while these mutations occur in diverse locations in the RNAP, they share a common adaptive mechanism. In turn, these findings highlight the resource allocation tradeoffs organisms face and suggest how the structure of the regulatory network enhances evolvability.

Graphical abstract

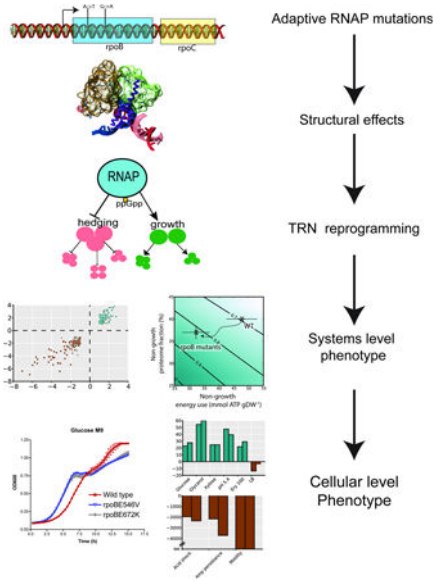

Introduction

Many causal genetic variants across all forms of life are found in regulatory regions (Enard et al., 2014; Fraser, 2013; Jones et al., 2012; King and Wilson, 1975; Prud'homme et al., 2007; Wray, 2007). In addition to *cis* regulatory variation, causal mutations are often found in *trans*-acting transcriptional regulators (Barrick et al., 2010; Ferenci, 2008; LaCroix et al., 2015; Sandberg et al., 2014; Saxer et al., 2014). Due to transcriptional regulators' involvement in multiple cellular processes, mutations in transcriptional regulators often affect multiple phenotypes (King et al., 2004; Solopova et al., 2014; Venturelli et al., 2015; Wang et al., 2015). Understanding the multi-scale and pleiotropic cascade of events resulting from regulatory mutations poses a challenge for systems biology.

Adaptive Laboratory Evolution (ALE) allows for adaptive mutations to be found and characterized in the context of clear selection pressures. ALE experiments repeatedly identify mutations in the RNA polymerase (RNAP)(Barrick et al., 2010; Dragosits et al., 2013; LaCroix et al., 2015; Sandberg et al., 2014; Tenaillon et al., 2012). Several of these mutations have been shown to result in fitness benefits in the selected environment and fitness deficits in several different environments (Cheng et al., 2014; Conrad et al., 2010; Dragosits et al., 2013). While the RNAP is not typically considered a transcription factor, it can be considered to lie at the top of the transcriptional regulatory network hierarchy. Presumably, these mutations alter the gene regulatory network to change the specific balance of cellular resources.

Here, we detail the multi-scale mechanism underlying several *trans*-acting adaptive regulatory mutations of *E. coli*'s RNAP (Cheng et al., 2014; Conrad et al., 2010; LaCroix et al., 2015). Using detailed phenotypic assays we show consistent fitness effects in different environments. A multi-'omic' approach with key environmental controls reveals a systematic and consistent modulation of the transcriptional regulatory network (TRN) towards growth functions and away from functions that hedge against environmental change. 'Econometric' analysis using a genome-scale model reveals that the resulting resource re-allocation can quantitatively explain the fitness effects. Finally, structural dynamics of RNA polymerase (RNAP) provide insight as to how these mutations result in strikingly similar effects. This study moves the field forward by detailing the multi-scale molecular, phenotypic, and physiological responses underlying the pleiotropic effects of adaptive regulatory mutations. It provides insight into the evolutionary constraints and the mechanisms that govern resource allocation in simple organisms.

Results

Pleiotropy of adaptive mutations in RNA polymerase

A recent adaptive laboratory evolution (ALE) experiment of *E. coli* in glucose minimal media (MM) identified recurring mutations in *rpoB* (the β subunit of RNAP), including *rpoB* E546V and *rpoB* E672K (LaCroix et al., 2015). We introduced these two ALE-selected mutations into the starting strain (i.e., the 'wild type' strain) and observed consistent physiological effects. Growth rate increased (by ∼25%) resulting from increases in both biomass yield (by ∼11%) and substrate uptake rate (by ∼14%). The use of an automated plate reader to obtain frequent measurements revealed a diauxic shift of the mutant strains in glucose M9 mineral media (Figure 1A).

Since mutations often have positive and negative fitness effects across several environments (referred to as pleiotropy), we then assessed the growth rate of the *rpoB* E546V and *rpoB* E672K mutants under a variety of single carbon sources, mixtures of carbon sources, rich media, and stress conditions. Additionally, we performed motility, acid shock, and antibiotic persistence phenotypic tests (Figure 1B and S1, Data S1-S2). These RNAP mutations show consistent fitness effects: they enable faster growth in several carbon sources, in low pH, and in the presence of erythromycin. However, they lead to lower motility, lower survival under acid shock, reduced antibiotic persistence, longer diauxic shifts, and lower growth rates in complex media.

Therefore, the mutants show increased fitness in conditions of steady-state growth, but a decreased fitness in changing environments. In other words, they show strong, consistent antagonistic pleiotropy for growth versus 'hedging' functions.

Mutations in RNA polymerase are highly specific

To assess whether other amino acid substitutions in the RNAP ALE-selected loci affect growth phenotypes, we used multiplex automated genome engineering (MAGE) (Wang et al., 2009) to generate variants in all possible 546 and 672 positions. After 8-12 rounds of MAGE we isolated and verified 6 variants of E546X position and 7 variants for the E672X

position. Two amino acid substitutions, E546K and E672R, which have similar chemical properties as those discovered by ALE, resulted in an increase in growth rate. These MAGE-selected mutants also exhibit longer diauxic shifts, showing similar pleiotropic effects as the ALE selected mutants (Figure S2). All other amino acid substitutions generated by MAGE did not affect growth rate significantly.

These results suggest that the mutations in RNAP affecting fitness are specific. Namely, all faster-growing RNAP mutants showed antagonistic pleiotropy for growth versus 'hedging'.

Genome-scale transcript profiling reveals conserved growth versus hedging response

To reveal the systems-level mechanism of the pleiotropic effects of the RNAP mutations, we obtained RNA-seq and metabolomics data from mid-logarithmic growth phase in glucose minimal media for the wild-type, *rpoB* E546V, and *rpoB* E672K mutant strains (Figure S3). The concentrations of 10 metabolites, including pyrimidine, glycolytic, and TCA intermediates, changed significantly compared to the wild-type (Student's t-test, $p < 0.01$, Bonferroni corrected). But overall, the metabolome remained fairly stable (Figure S3, Data S1). In contrast, the expression profiling data revealed 243 consistently differentially expressed genes. Like the pleiotropic fitness effects of the mutants, the differential gene expression is strikingly consistent (Figure 2A, left), suggesting a common underlying mechanism at the systems level.

Notably, we also found that the differential expression profiles of the two strains harboring *rpoB* mutants were similar to that of a previously profiled mutant strain that has a 27 amino acid deletion in the β′ subunit of the RNAP (*rpoC*-del27, identified by ALE on glycerol) (Cheng et al., 2014; Conrad et al., 2010; Herring et al., 2006). The changes in expression of the *rpoC*-del27 mutant (Cheng et al., 2014) (compared to wild-type) grown in glycerol match those of the *rpoB* mutants grown in glucose (Figure 2A, right; χ^2 test for independence, $p < 10^{-8}$).

To obtain insight into the processes perturbed by the RNAP mutations, we classified the 243 consistently differentially expressed genes by function (Data S3). We found that the genes in the same functional category are often differentially expressed in a consistent direction. We used this observation to define up-regulated and down-regulated functions. The up-regulated functions (defined as >80% of the genes being up-regulated) were broadly related to cellular growth, including protein synthesis and folding, amino acid biosynthesis and uptake, and carbohydrate transport and utilization. On the other hand, the down-regulated functions (defined as >80% of the genes being down-regulated) broadly hedge against environmental change and stress, including osmotic and oxidative stress, flagella, chemotaxis, acid resistance, and biofilm formation. Two categories of genes were not consistently up or down-regulated; these are DNA repair and genes with unknown function. Some of the differentially expressed genes were transcription factors or small RNA regulators (Figure 4B). These regulators were differentially expressed in the direction expected based on the directionality of the regulator (i.e, activator or repressor) and the direction of the differential expression of the regulated functional category (Data S3, Table S3). Thus, at the molecular level, the differentially expressed genes reflect the growth versus hedging phenotypes observed at the organismal level.

Environmental controls disentangle cause versus effect of mutations

As growth rate itself has a strong effect on gene expression (Klumpp and Hwa, 2014), we sought to identify the differential expression changes caused only by the mutation from those caused indirectly by increased growth. To disentangle these effects, we obtained RNA-seq data under conditions where the wild-type and mutant strains grow at the same rate (glucose limited chemostat culture) and under conditions where the mutants grow slower than the wild-type (LB rich media). Regardless of the growth rate and environment, the hedging functions were down-regulated in the mutant strain compared to the wild-type (Figure 2C). Differential expression of the growth functions, however, was dependent on the growth rate: growth genes were not differentially expressed in chemostat and were down-regulated in LB. Thus, these environmental controls disentangle the cause and effect of the mutations: the mutations directly result in the down-regulation of hedging genes whereas expression of the growth-related genes is coupled to the cell's growth rate.

Structural dynamics of RNAP suggests a common allosteric mechanism

Both mutations, *rpoB* E546V and E672K, are located ∼25 Å from the catalytic site of RNAP, and ∼25 Å from each other. How do they result in such similar patterns in transcriptional reprogramming to down-regulate hedging functions?

To investigate this question, we performed molecular dynamics simulations of the core RNAP open complex aiming to propose a common putative molecular mechanism for the pleiotropic fitness effects of the *rpoB* mutations. We found a strong correlation between the extent of increase in interaction energy between the β and β′ subunits, and the increase in cell fitness for various E672 mutations generated by MAGE (both beneficial and neutral, Figure 3A). Such destabilization of subunit interaction is consistent with a previous study that showed a decrease in open complex half-life of the *rpoC*-del27 mutation, which has similar growth and transcriptional effects (Conrad et al., 2010).

To further explore the functional correlation among different mutations, we decomposed the RNAP complex into ∼20 ‘structural communities’ within which the molecular motions of residues are strongly correlated (Sethi et al., 2009). Despite the large spatial separation between E672 and E546, they belong to the same dynamical community (Figure 3B). Furthermore, many mutations detected in RNAP in other ALE experiments (Barrick et al., 2010; LaCroix et al., 2015; Tenaillon et al., 2012) can also be found in this and neighboring communities (Figure 3B and Table S4). This structural community consists of ∼250 residues in *rpoB*, part of the bridge helix (BH) in *rpoC*, and nucleotides on the template DNA strand. As such, we may link the collective motions of these structural modules to the structural rearrangements of BH that were shown to coordinate catalysis and DNA translocation in the nucleotide addition cycle (NAC) (Bar-Nahum et al., 2005; Weinzierl, 2010).

Three observations about the motions of structural modules in RNAP are notable. First, the bridge helix kinked at two hinge positions (BH-H_N and BH-H_C, Figure 3C) in discrete steps of ∼10° to 20°, indicating the existence of transient metastable intermediates between the RNAP open and close conformations. Second, boundary between the two neighboring

structural communities switched from BH-H_N to BH-H_C when the BH went through transition from its bent to relaxed state. Third, there was a strong correlation between the bending angle of the BH and the relative motion between neighboring communities along the direction of DNA translocation. Based on these observations, we hypothesize that the ALE-selected mutations may modulate the stability of the RNAP open complex by adjusting the coupling between the relative motions of neighboring communities and the bending-relaxing cycle of the BH (Figure 3C).

The stability of the RNAP open complex not only affects efficiency of the nucleotide elongation reactions, but may also modulate the multistep process of bacterial transcription initiation (Saecker et al., 2011). First, it has been shown that the competitive binding of different σ factors to the RNAP core enzyme can be tuned by the stability of open complex in the presence of (p)ppGpp or σ^D mutations (Barker et al., 2001; Jishage et al., 2002; Osterberg et al., 2011). Notably, many RNAP mutations with experimentally measured short-lived open complex are located in community 1, indicating that E672 and E546 (and other ALE-selected mutations in the same and neighboring community, Figure 3B) may achieve global transcriptional regulation in a similar way. Second, further along the transcription initiation process, lower stability of the open complex is shown to facilitate σ factor release and promoter escape which in turn coordinate the probability of abortive and productive RNA synthesis (Cashel et al., 2003; Roberts and Roberts, 1996). It is worth noting that sequence and structural differences in the critical $\sigma_{3.2}$ region of σ^D and σ^S may be coupled to open complex stability in order to convey differential transcription regulation for growth-related versus hedging functions.

In summary, we observed a strong correlation between the open complex stability and the growth rates of RNAP mutants. Detailed analysis of the structural communities suggested a common molecular mechanism, regarding how distantly located mutations may result in the same allosteric effect. Although previous findings indicated that open complex stability can modulate global transcription through alternative σ factors binding, coordination of abortive RNA synthesis, and speed of nucleotide addition, further experiments are required to draw conclusion on the exact mechanism as to how the ALE-selected mutations achieve these goals.

Transcriptional regulatory network perturbation explains observed molecular response

Consistent with the perturbed structural properties of the mutated RNAP, the down-regulated (hedging) genes tend to have promoters utilizing stress related sigma factors (σ^S, σ^F), and the up-regulated (growth) genes tend to have promoters utilizing growth related sigma factors (σ^D, σ^N, σ^H) (Figure 4A and S4). The sigma factors themselves are not detectably differentially expressed. However, the observed differential expression is more specific than that caused by sigma factors alone.

There are 10 transcription factors (TFs) and regulatory small RNAs (sRNAs) that were differentially expressed in the mutant strains (Figure 4B). Each of these regulators can be associated with one or more of the differentially expressed functional categories identified (Table S3). Furthermore, across all of the strains (wild-type, *rpoB* E546V, and *rpoB* E672K) and environments (glucose excess, glucose limitation, and rich media) examined with RNA-

seq, the differential expression of the identified growth and hedging functions was in a direction consistent with the differential expression of their regulators (based on known activation or repression relationships; Figure 4B). Taken together, these results suggest that the balance between growth and hedging functions is achieved through global modulation of the transcriptional regulatory network. The structure of the network may enable *E. coli* to rebalance its proteome in response to evolutionary pressures with single point mutations in RNAP.

'Econometric' analysis of proteome and energy resource allocation explains the fitness trade-off

The molecular and regulatory effects of the *rpoB* mutations revealed that resource allocation underlies the observed growth versus hedging fitness effects. We used a recently developed genome-scale computer model of microbial growth (O'Brien et al., 2013), called a ME-model (Lerman et al., 2012; Liu et al., 2014; O'Brien et al., 2013; Thiele et al., 2009) (for metabolism and expression) to quantify the fitness effects associated with proteome and energy reallocation by these mutations (Figure 5A).

The ME-model allows global energy accounting based on the physiological data from wild-type and RNAP mutant strains. This analysis showed that the RNAP mutations shift about a third (28-37%) of the unaccounted for energy (i.e., processes outside of metabolism and protein synthesis, often referred to as the 'maintenance energy' (Pirt, 1982)) to growth related processes (Figure 5B). Then, using the gene expression data, we estimated a 2-5% reduction of the transcriptome allocated to non-ME genes (i.e., genes not included in the ME-model; non-growth functions) and a commensurate increase in allocation to ME genes (i.e., modeled, growth functions) in the RNAP mutants (Figure 5B). ME-model analysis thus shows a clear shift to a more growth-supporting energy and proteome allocation as a result of the observed RNAP mutations.

We used the ME-model to understand how these changes in resource allocation affect cellular physiology (i.e., growth rate, biomass yield, and uptake rate). The non-ME proteome and energy allocation are adjustable model variables; when varied in the model, the measured changes in non-ME energy and transcriptome allocation can quantitatively account for the measured physiological changes (biomass yield and uptake rate) in the mutant strains (Figure 5C and S5). Therefore, the growth increase can be accounted for by the measured change in resource allocation, suggesting that the expression of hedging functions restrains growth rate in the wild-type strain.

The ME-model allowed us to quantitatively elucidate the relationship between changes in overall physiological measures (i.e., growth rate, substrate uptake rate, and yield) and the changes in allocation of protein and energy (Figure 5). On the basis of this quantitative relationship, we suggest that the pleiotropic effects of the *rpoB* mutation are due to a fundamental constraint of limited proteome and energy resources, leading to an inherent trade-off in resource allocation.

Discussion

Here, we elucidate the mechanistic multi-scale phenotypic effects of adaptive regulatory mutations. Single amino acid changes in the RNAP reprogram the transcriptional regulatory network to re-allocate resources towards growth and away from hedging functions. The mutations result in antagonistic pleiotropy where the organism is more fit in stable environments but less fit in environmental shifts and shocks (Futuyma and Moreno, 1988).

Antagonistic pleiotropy due to a fundamental trade-off

Mutations that are beneficial or neutral in one environment often have negative fitness effects in other environments, referred to as pleiotropy. Pleiotropy shapes the evolution of organisms and is thought to underlie the evolution of specialist species. Several mechanisms can give rise to pleiotropy and some have been demonstrated (Cooper and Lenski, 2000; Leiby and Marx, 2014; Remold, 2012).

Fundamental biological constraints can result in antagonistic pleiotropy, though examples of these cases are lacking. Using a systems biology approach, we show that the growth rate difference in wild-type and mutant strains can be quantitatively explained by changes in proteome and energy allocation. These resources are limited, resulting in an inherent trade-off between growth and hedging functions. Such proteome and energy allocation constraints likely result in pervasive evolutionary trade-offs and likely underlie several recent examples of antagonistic pleiotropy (Solopova et al., 2014; Venturelli et al., 2015; Wang et al., 2015)..

Bacterial evolvability through regulatory network structure

Mounting evidence supports that much of the functional divergence between organisms occurs in regulatory regions (Enard et al., 2014; Fraser, 2013; Jones et al., 2012; King and Wilson, 1975; Prud'homme et al., 2007; Wray, 2007). The detailed example of the RNAP mutations here suggests why (in part) this may be the case.

As regulatory networks are ‘aligned’ with particular functional subsystems, mutations that perturb them change phenotypes in a functionally coherent manner (Innocenti and Chenoweth, 2013; Saxer et al., 2014; Wagner et al., 2007). The regulatory rebalancing detailed here occurs along a coherent growth versus hedging trajectory. On the other hand, mutations that are inconsistent or imbalanced in the molecular changes they cause would likely not be selected. Therefore, in addition to enabling short-term responses to environmental change, the structure of the regulatory network also enables longer-term productive evolutionary change. Remarkably, single, but non-unique, point mutations allow such adaptation.

Multi-scale characterization of genotype to phenotype

Sequencing of many individual genomes has led to the identification of genomic regions under selection (Grossman et al., 2013) and enabled the association of variants with organismal (McCarthy et al., 2008) and molecular (Cookson et al., 2009) phenotypes. However, there is a large gap between identifying causal variants and mechanistically understanding their phenotypic consequences. The mutations studied here are some of the

most comprehensively phenotyped to date, with environmental controls to separate cause and effect. We employ state-of-the-art structural and systems biology modeling approaches to help bridge the gap between genotype and phenotype. Together, these analysis approaches enabled us to infer links from mutation to biophysical effects on protein function to systems-level molecular and regulatory response, and finally to organismal phenotype (Figure 6). Therefore, this study outlines how we might begin to understand the multi-scale genotype-phenotype relationship at a true systems level.

Experimental Procedures

Strains and cultivations—*E. coli* MG1655 was used as wild-type. The ALE selected rpoBE564V and rpoBE672K knock in strains were previously constructed by allelic replacement (LaCroix et al., 2015). To generate additional variants of *rpoB* 546 and 672 positions, MAGE was performed on the wild-type strain by first transformation of recombineering plasmid pKD46 (Datsenko and Wanner, 2000), then inactivation of *mutS* with two nonsense mutations at residues 189 and 191 using an oligo (mutS_MUT). Two oligos (rpoB_E546X and rpoB_E672X) that resulted in NNS codon mutations at *rpoB* residues 546 and 672 were introduced into the strain through 8-12 rounds of MAGE, followed by colony isolation of mutants, PCR verification, and Sanger sequencing. To perform each cycle of MAGE, the λ-Red system was induced with 0.5%-arabinose 45 minutes prior to generation of electrocompetent cells and oligo. Batch cultures were done in flask with M9 minimal media and 4 g/L of glucose at 37°C or LB rich media. Glucose limited chemostats were carried out in a Bioflo 110 fermentor (New Brunswick Scientific, NJ). Glucose supplemented M9 was added to the reactor at 0.31 and 0.44 h^{-1} dilution rates controlled by a peristaltic pump. Steady state was achieved after 3-5 residence times and was verified by biomass measurements. Phenotypic tests were performed by inoculation of media with an overnight pre-culture of glucose M9 media for all cases. Erythromycin was added to the media to the indicated concentration. The pH of M9 was adjusted to the indicated value with 6M HCl. Different substrates and mixtures were added to M9 to test growth in the indicated conditions. All growth curves were inoculated to a 0.02 OD and 200 μL were cultured by triplicate in a Bioscreen C device at 37°C for 15- 24 h. Growth rates were calculated by determining the slope of the log-linear region using a linear regression, the first growth phase was used to do calculations when diauxic growth was observed.

Motility test—Cells were grown to mid log phase and 10 microliters of cell suspension were spotted onto 0.3% agar plate with glucose M9 media, plates were photographed motility was determined by halo expansion between 24 and 48h

Acid shock—Cells were harvested in mid log phase and normalized to 1×10^8 cells/mL, 50 μL of cells suspension were diluted in 950 μL of pH 2.6 glucose M9 media. After 3 hours of incubation cells were diluted and plated in LB agar plates for cell counts (Tucker et al., 2003).

Antibiotic persistence—Cells were harvested in mid log phase and normalized to 1×10^8 cells/mL, different dilutions were plated in LB ampicillin plates after 24h a sterile solution of 25 U of penicinillase was plated and plates were re-incubated for 24h. Appearance of

colonies was determined and persistence frequency determined in base of initial cell counts (Korch et al., 2003).

Analytics—Biomass was determined by measuring the absorbance of the culture at 600nm using an equivalence of 0.429gDW/L per OD_{600} unit. Glucose, and acetate were measured by HPLC using refractive index (RI) detection by high-performance liquid chromatography (HPLC) (Waters, MA) with a Bio-Rad Aminex HPX87-H ion exclusion column (injection volume, 10 μl) and 5mM H_2SO_4 as the mobile phase (0.5 ml/min, 45°C). Metabolomic sampling, extraction and analysis was carried out as described earlier by our group (McCloskey et al., 2015; McCloskey et al., 2014). At-test was performed on log-normalized data with metaboanalyst 3.0 suite (Xia et al., 2015) comparing the wild type to each of the mutants, a p-value cutoff of 0.01 and Bonferroni correction was used to determine significance between metabolite concentration levels.

RNA-seq libraries—Samples for RNA-sequencing were taken in mid log phase of batch cultures or during the steady-state in chemostats. Cells were collected with Qiagen RNA-protect Bacteria Reagent and pelleted for storage at -80°C prior to RNA extraction. Cell pellets were thawed and incubated with Readylyse Lysozyme, SuperaseIn, Protease K, and 20% SDS for 20 minutes at 37°C. Total RNA was isolated and purified using the Qiagen RNeasy Mini Kit columns and following vendor procedures. An on-column DNase-treatment was performed for 30 minutes at room temperature. RNA was quantified using a Nano drop and quality assessed by running an RNA-nano chip on a bioanalyzer. The rRNA was removed using Epicentre's Ribo-Zero rRNA removal kit for Gram Negative Bacteria. Paired-end, strand-specific RNA-seq was performed following a modified dUTP method (Latif et al., 2013).

Transcriptome analyses—The obtained reads were mapped to the *E. coli* MG1655 genome (NC_000913.2) using the short-read aligner Bowtie (http://bowtie-bio.sourceforge.net) (Langmead, 2010) with two mismatches allowed per read alignment. To estimate gene expression FPKM values were calculated using cufflinks tool and differential expression analysis was carried out using cuffdiff feature of the same package using the upper quartile normalization (http://cufflinks.cbcb.umd.edu/) (Trapnell et al., 2010).

Regulatory network—Sigma factor use at promoters was obtained by combining annotations in Cho et al. (Cho et al., 2014) and EcoCyc (Keseler et al., 2013). The list of all transcription factors and sRNAs was obtained from RegulonDB (Salgado et al., 2013). A two-proportion z-test with two-tailed comparisons was used to determine significant differences in sigma factor usage among up-regulated and down-regulated genes.

Computation of maximum non-growth energy use—The *E. coli* ME-Model with all parameters as published in O'Brien et al. was used (O'Brien et al., 2013). For all replicate cultivations, the measured growth rate, glucose uptake rate, and acetate secretion rate were fixed in the model. The maximum unaccounted for energy use was then computed by maximizing the flux through ATP maintenance reaction, which hydrolyzes ATP. For a given strain, the unaccounted for energy use is reported as the average across biological replicates.

Computation of non-ME transcriptome—The (protein coding) ME and non-ME transcriptome fractions were estimated using FPKM and gene length. A gene's transcriptome fraction was taken to be the product of FPKM and the gene length, divided by the sum of this product over all genes. The ME and non-ME transcriptome fractions were then calculated by summing the transcriptome fractions of all ME and non-ME genes, respectively. Ranges are determined from the estimated lower and upper FPKM values across different samples.

Computation of the effects of changes in resource allocation—Protein and energy that are not used towards cell growth are changeable variables in the ME-Model. These are varied to determine the growth rate, biomass yield, and substrate uptake rate contours (Figure 5C, S5). The points and error bars for wild-type and *rpoB* mutants are placed according to the unaccounted for energy (Figure 5C) and change in non-ME transcriptome (Figure 5B). As we do not explicitly know the proteome fraction devoted to growth in each strain, we determine these values with two assumptions. First, we assume the change in non-growth proteome is equal to the change in the non-ME transcriptome. Second, we infer the non-growth proteome in the wild-type strain based on its measured growth (which is why there is no y-axis error bar for the wild-type), resulting in a value consistent with previous estimates (Scott et al., 2010).

Molecular dynamics simulations—Molecular model of the *E. coli* RNAP elongation complex (EC) were created using the crystal structure of the *E. coli* RNAP core enzymes (PDB code: 3LU0 (Opalka et al., 2010), the template and non-template DNA strands, and the DNA:RNA hybrid helix (PDB code: 2O5J (Vassylyev et al., 2007). The model represented the open conformation of RNAP EC, and we model selected substrates into the active site to mimic the pre-translocated state (with ADE), the post-translocated state (no additional substrate), and the post-translocated preinsertion state (with ATP) during the nucleotide elongation cycle.

All three systems were neutralized with Mg^{2+} and K^{+} ions, initially placed in positions occupied by metal ions in the crystal structure or according to the electrostatic potential. The complexes were then solvated by well-equilibrated water molecules with periodic boundary conditions. 200 mM KCl was added to the final solution. Minimization and equilibration were conducted by releasing constraints step-by-step according to the protocol described in (Eargle and Luthey-Shulten, 2012; Lai et al., 2013). Such procedure was shown to be critical to maintain stability of complex molecular system with interactions between protein, RNA and DNA. Production runs were performed with 1-fs time step under constant pressure (1 atm) and constant temperature (25 °C) using NAMD2.9 (Phillips et al., 2005) and the CHARMM36 force field (Best et al., 2012) A total of 140 ns MD simulations of the RNAP open complex were obtained for analysis, including 50 ns from the pre-translocated state, 60 ns from the pre-translocated state, and 30 ns from the pre-translocated preinserted state.

Analysis of the molecular dynamics trajectory—Analysis of the three MD trajectories showed consistent results. Therefore we present the results from the longest simulation of post-translocated state as the representative.

Interaction energy change between the β and β′ subunits upon mutations were calculated with the alanine scan script using PyRosetta (Chaudhury et al., 2010) originally distributed by the Gray lab (http://graylab.jhu.edu/pyrosetta/downloads/pyrosetta_scripts/ala_scan.zip). We applied modifications of the score function parameterized according to recently reported protocols (Gavenonis et al., 2014; Kortemme and Baker, 2002). To reduce the bias introduced by a single static crystal structure, we performed the computational alanine scan every 25 ps through the entire trajectories, resulting in a broad distribution of the ddG values. Although such ddG value was taken to be qualitative conventionally (with ddG > 1 kcal/mol to be destabilizing), we emphasized that it was the observed trend over the dynamical trajectory that correlated with phenotypic fitness of the MAGE mutants.

Dynamical community analysis was done using algorithms described in (Sethi et al., 2009) with the NetworkView plugin (Eargle and Luthey-Shulten, 2012) in VMD (Humphrey et al., 1996). The analysis was done for two chosen windows (3-23 ns and 35-55 ns) in the 60 ns trajectory of the post-translocated state, because the overall RMSD of the RNAP complex suggested that they might represent two different conformations during the RNAP EC open-close conformational transition.

Supplementary Material

Refer to Web version on PubMed Central for supplementary material.

Acknowledgments

We thank Richard Szubin for technical assistance and Markus Herrgard and Elizabeth Brunk for valuable discussions. The Novo Nordisk Foundation supported this work. EJO was supported by NIH GM057089. This research used resources of the National Energy Research Scientific Computing Center, which is supported by the Office of Science of the U.S. Department of Energy under Contract No. DE-AC02-05CH11231.

References

Bar-Nahum G, Epshtein V, Ruckenstein AE, Rafikov R, Mustaev A, Nudler E. A ratchet mechanism of transcription elongation and its control. Cell. 2005; 120:183–193. [PubMed: 15680325]

Barker MM, Gaal T, Gourse RL. Mechanism of regulation of transcription initiation by ppGpp. II. Models for positive control based on properties of RNAP mutants and competition for RNAP. Journal of molecular biology. 2001; 305:689–702. [PubMed: 11162085]

Barrick JE, Kauth MR, Strelioff CC, Lenski RE. Escherichia coli rpoB mutants have increased evolvability in proportion to their fitness defects. Molecular biology and evolution. 2010; 27:1338–1347. [PubMed: 20106907]

Best RB, Zhu X, Shim J, Lopes PE, Mittal J, Feig M, Mackerell AD Jr. Optimization of the additive CHARMM all-atom protein force field targeting improved sampling of the backbone phi, psi and side-chain chi(1) and chi(2) dihedral angles. J Chem Theory Comput. 2012; 8:3257–3273. [PubMed: 23341755]

Cashel M, Hsu LM, Hernandez VJ. Changes in conserved region 3 of Escherichia coli sigma 70 reduce abortive transcription and enhance promoter escape. J Biol Chem. 2003; 278:5539–5547. [PubMed: 12477716]

Chaudhury S, Lyskov S, Gray JJ. PyRosetta: a script-based interface for implementing molecular modeling algorithms using Rosetta. Bioinformatics. 2010; 26:689–691. [PubMed: 20061306]

Cheng KK, Lee BS, Masuda T, Ito T, Ikeda K, Hirayama A, Deng L, Dong J, Shimizu K, Soga T, et al. Global metabolic network reorganization by adaptive mutations allows fast growth of Escherichia coli on glycerol. Nat Commun. 2014; 5:3233. [PubMed: 24481126]

Cho BK, Kim D, Knight EM, Zengler K, Palsson BO. Genome-scale reconstruction of the sigma factor network in Escherichia coli: topology and functional states. BMC Biol. 2014; 12:4. [PubMed: 24461193]

Conrad TM, Frazier M, Joyce AR, Cho BK, Knight EM, Lewis NE, Landick R, Palsson BO. RNA polymerase mutants found through adaptive evolution reprogram Escherichia coli for optimal growth in minimal media. P Natl Acad Sci USA. 2010; 107:20500–20505.

Cookson W, Liang L, Abecasis G, Moffatt M, Lathrop M. Mapping complex disease traits with global gene expression. Nature reviews Genetics. 2009; 10:184–194.

Cooper VS, Lenski RE. The population genetics of ecological specialization in evolving Escherichia coli populations. Nature. 2000; 407:736–739. [PubMed: 11048718]

Datsenko KA, Wanner BL. One-step inactivation of chromosomal genes in Escherichia coli K-12 using PCR products. Proc Natl Acad Sci U S A. 2000; 97:6640–6645. [PubMed: 10829079]

Dragosits M, Mozhayskiy V, Quinones-Soto S, Park J, Tagkopoulos I. Evolutionary potential, cross-stress behavior and the genetic basis of acquired stress resistance in Escherichia coli. Mol Syst Biol. 2013; 9:1–13.

Eargle, J.; Luthey-Shulten, Z. Simulating Dynamics in RNA-Protein Complexes. In: L, N.; Westhof, E., editors. RNA 3D structure Analysis and Prediction. Nucleic Acids and Molecular Biology, Springer-Verlag Berlin Heidelberg; 2012.

Enard D, Messer PW, Petrov DA. Genome-wide signals of positive selection in human evolution. Genome Research. 2014; 24:885–895. [PubMed: 24619126]

Ferenci T. The spread of a beneficial mutation in experimental bacterial populations: the influence of the environment and genotype on the fixation of rpoS mutations. Heredity. 2008; 100:446–452. [PubMed: 18073783]

Fraser HB. Gene expression drives local adaptation in humans. Genome Research. 2013; 23:1089–1096. [PubMed: 23539138]

Futuyma DJ, Moreno G. The Evolution of Ecological Specialization. Annu Rev Ecol Syst. 1988; 19:207–233.

Gavenonis J, Sheneman BA, Siegert TR, Eshelman MR, Kritzer JA. Comprehensive analysis of loops at protein-protein interfaces for macrocycle design. Nat Chem Biol. 2014; 10:716–722. [PubMed: 25038791]

Grossman SR, Andersen KG, Shlyakhter I, Tabrizi S, Winnicki S, Yen A, Park DJ, Griesemer D, Karlsson EK, Wong SH, et al. Identifying recent adaptations in large-scale genomic data. Cell. 2013; 152:703–713. [PubMed: 23415221]

Herring CD, Raghunathan A, Honisch C, Patel T, Applebee MK, Joyce AR, Albert TJ, Blattner FR, van den Boom D, Cantor CR, et al. Comparative genome sequencing of Escherichia coli allows observation of bacterial evolution on a laboratory timescale. Nature genetics. 2006; 38:1406–1412. [PubMed: 17086184]

Humphrey W, Dalke A, Schulten K. VMD: visual molecular dynamics. J Mol Graph. 1996; 14:33–38. 27–38. [PubMed: 8744570]

Innocenti P, Chenoweth SF. Interspecific divergence of transcription networks along lines of genetic variance in Drosophila: dimensionality, evolvability, and constraint. Molecular biology and evolution. 2013; 30:1358–1367. [PubMed: 23519314]

Jishage M, Kvint K, Shingler V, Nystrom T. Regulation of sigma factor competition by the alarmone ppGpp. Genes Dev. 2002; 16:1260–1270. [PubMed: 12023304]

Jones FC, Grabherr MG, Chan YF, Russell P, Mauceli E, Johnson J, Swofford R, Pirun M, Zody MC, White S, et al. The genomic basis of adaptive evolution in threespine sticklebacks. Nature. 2012; 484:55–61. [PubMed: 22481358]

Keseler IM, Mackie A, Peralta-Gil M, Santos-Zavaleta A, Gama-Castro S, Bonavides-Martinez C, Fulcher C, Huerta AM, Kothari A, Krummenacker M, et al. EcoCyc: fusing model organism databases with systems biology. Nucleic Acids Res. 2013; 41:D605–612. [PubMed: 23143106]

King MC, Wilson AC. Evolution at two levels in humans and chimpanzees. Science. 1975; 188:107–116. [PubMed: 1090005]

King T, Ishihama A, Kori A, Ferenci T. A Regulatory Trade-Off as a Source of Strain Variation in the Species Escherichia coli A Regulatory Trade-Off as a Source of Strain Variation in the Species Escherichia coli †. 2004; 186:5614–5620.

Klumpp S, Hwa T. Bacterial growth: global effects on gene expression, growth feedback and proteome partition. Current opinion in biotechnology. 2014; 28C:96–102. [PubMed: 24495512]

Korch SB, Henderson TA, Hill TM. Characterization of the hipA7 allele of Escherichia coli and evidence that high persistence is governed by (p)ppGpp synthesis. Mol Microbiol. 2003; 50:1199–1213. [PubMed: 14622409]

Kortemme T, Baker D. A simple physical model for binding energy hot spots in protein-protein complexes. Proc Natl Acad Sci U S A. 2002; 99:14116–14121. [PubMed: 12381794]

LaCroix RA, Sandberg TE, O'Brien EJ, Utrilla J, Ebrahim A, Guzman GI, Szubin R, Palsson BO, Feist AM. Use of adaptive laboratory evolution to discover key mutations enabling rapid growth of Escherichia coli K-12 MG1655 on glucose minimal medium. Appl Environ Microbiol. 2015; 81:17–30. [PubMed: 25304508]

Lai J, Chen K, Luthey-Schulten Z. Structural intermediates and folding events in the early assembly of the ribosomal small subunit. J Phys Chem B. 2013; 117:13335–13345. [PubMed: 23972210]

Langmead B. Aligning short sequencing reads with Bowtie. Curr Protoc Bioinformatics. 2010; Chapter 11 Unit 11 17.

Latif H, Lerman JA, Portnoy VA, Tarasova Y, Nagarajan H, Schrimpe-Rutledge AC, Smith RD, Adkins JN, Lee DH, Qiu Y, et al. The genome organization of Thermotoga maritima reflects its lifestyle. PLoS Genet. 2013; 9:e1003485. [PubMed: 23637642]

Leiby N, Marx CJ. Metabolic erosion primarily through mutation accumulation, and not tradeoffs, drives limited evolution of substrate specificity in Escherichia coli. PLoS biology. 2014; 12:e1001789. [PubMed: 24558347]

Lerman JA, Hyduke DR, Latif H, Portnoy VA, Lewis NE, Orth JD, Schrimpe-Rutledge AC, Smith RD, Adkins JN, Zengler K, et al. In silico method for modelling metabolism and gene product expression at genome scale. Nature communications. 2012; 3:929–929.

Liu JK, O'Brien EJ, Lerman Ja, Zengler K, Palsson BO, Feist AM. Reconstruction and modeling protein translocation and compartmentalization in Escherichia coli at the genome-scale. BMC Systems Biology. 2014; 8:110–110. [PubMed: 25227965]

McCarthy MI, Abecasis GR, Cardon LR, Goldstein DB, Little J, Ioannidis JP, Hirschhorn JN. Genome-wide association studies for complex traits: consensus, uncertainty and challenges. Nature reviews Genetics. 2008; 9:356–369.

McCloskey D, Gangoiti JA, Palsson BO, Feist AM. A pH and solvent optimized reverse-phase ion-paring-LC-MS/MS method that leverages multiple scan-types for targeted absolute quantification of intracellular metabolites. Metabolomics. 2015; 11:1338–1350.

McCloskey D, Utrilla J, Naviaux RK, Palsson BO, Feist AM. Fast Swinnex filtration (FSF): a fast and robust sampling and extraction method suitable for metabolomics analysis of cultures grown in complex media. Metabolomics. 2014; 11:198–209.

O'Brien EJ, Lerman JA, Chang RL, Hyduke DR, Palsson BO. Genome-scale models of metabolism and gene expression extend and refine growth phenotype prediction. Mol Syst Biol. 2013; 9:693. [PubMed: 24084808]

Opalka N, Brown J, Lane WJ, Twist KA, Landick R, Asturias FJ, Darst SA. Complete structural model of Escherichia coli RNA polymerase from a hybrid approach. PLoS Biol. 2010; 8

Osterberg S, del Peso-Santos T, Shingler V. Regulation of alternative sigma factor use. Annu Rev Microbiol. 2011; 65:37–55. [PubMed: 21639785]

Phillips JC, Braun R, Wang W, Gumbart J, Tajkhorshid E, Villa E, Chipot C, Skeel RD, Kale L, Schulten K. Scalable molecular dynamics with NAMD. J Comput Chem. 2005; 26:1781–1802. [PubMed: 16222654]

Pirt SJ. Maintenance energy: a general model for energy-limited and energy-sufficient growth. Arch Microbiol. 1982; 133:300–302. [PubMed: 7171288]

Prud'homme B, Gompel N, Carroll SB. Emerging principles of regulatory evolution. P Natl Acad Sci USA. 2007; 104 Suppl 1:8605–8612.

Remold S. Understanding specialism when the Jack of all trades can be the master of all. Proc Biol Sci. 2012; 279:4861–4869. [PubMed: 23097515]

Roberts CW, Roberts JW. Base-specific recognition of the nontemplate strand of promoter DNA by E. coli RNA polymerase. Cell. 1996; 86:495–501. [PubMed: 8756731]

Saecker RM, Record MT Jr, Dehaseth PL. Mechanism of bacterial transcription initiation: RNA polymerase - promoter binding, isomerization to initiation-competent open complexes, and initiation of RNA synthesis. J Mol Biol. 2011; 412:754–771. [PubMed: 21371479]

Salgado H, Peralta-Gil M, Gama-Castro S, Santos-Zavaleta A, Muniz-Rascado L, Garcia-Sotelo JS, Weiss V, Solano-Lira H, Martinez-Flores I, Medina-Rivera A, et al. RegulonDB v8.0: omics data sets, evolutionary conservation, regulatory phrases, cross-validated gold standards and more. Nucleic Acids Res. 2013; 41:D203–213. [PubMed: 23203884]

Sandberg TE, Pedersen M, LaCroix RA, Ebrahim A, Bonde M, Herrgard MJ, Palsson BO, Sommer M, Feist AM. Evolution of Escherichia coli to 42 degrees C and Subsequent Genetic Engineering Reveals Adaptive Mechanisms and Novel Mutations. Mol Biol Evol. 2014; 31:2647–2662. [PubMed: 25015645]

Saxer G, Krepps MD, Merkley ED, Ansong C, Deatherage Kaiser BL, Valovska MT, Ristic N, Yeh PT, Prakash VP, Leiser OP, et al. Mutations in global regulators lead to metabolic selection during adaptation to complex environments. PLoS Genet. 2014; 10:e1004872. [PubMed: 25501822]

Scott M, Gunderson CW, Mateescu EM, Zhang Z, Hwa T. Interdependence of cell growth and gene expression: origins and consequences. Science. 2010; 330:1099–1102. [PubMed: 21097934]

Sethi A, Eargle J, Black AA, Luthey-Schulten Z. Dynamical networks in tRNA:protein complexes. Proc Natl Acad Sci U S A. 2009; 106:6620–6625. [PubMed: 19351898]

Solopova A, van Gestel J, Weissing FJ, Bachmann H, Teusink B, Kok J, Kuipers OP. Bet-hedging during bacterial diauxic shift. Proc Natl Acad Sci U S A. 2014; 111:7427–7432. [PubMed: 24799698]

Tenaillon O, Rodriguez-Verdugo A, Gaut RL, McDonald P, Bennett AF, Long AD, Gaut BS. The molecular diversity of adaptive convergence. Science. 2012; 335:457–461. [PubMed: 22282810]

Thiele I, Jamshidi N, Fleming RM, Palsson BO. Genome-scale reconstruction of Escherichia coli's transcriptional and translational machinery: a knowledge base, its mathematical formulation, and its functional characterization. PLoS Comput Biol. 2009; 5:e1000312. [PubMed: 19282977]

Trapnell C, Williams BA, Pertea G, Mortazavi A, Kwan G, van Baren MJ, Salzberg SL, Wold BJ, Pachter L. Transcript assembly and quantification by RNA-Seq reveals unannotated transcripts and isoform switching during cell differentiation. Nat Biotechnol. 2010; 28:511–515. [PubMed: 20436464]

Tucker DL, Tucker N, Ma Z, Foster JW, Miranda RL, Cohen PS, Conway T. Genes of the GadX-GadW regulon in Escherichia coli. J Bacteriol. 2003; 185:3190–3201. [PubMed: 12730179]

Vassylyev DG, Vassylyeva MN, Zhang J, Palangat M, Artsimovitch I, Landick R. Structural basis for substrate loading in bacterial RNA polymerase. Nature. 2007; 448:163–168. [PubMed: 17581591]

Venturelli OS, Zuleta I, Murray RM, El-Samad H. Population Diversification in a Yeast Metabolic Program Promotes Anticipation of Environmental Shifts. PLOS Biology. 2015; 13:e1002042–e1002042. [PubMed: 25626086]

Wagner GP, Pavlicev M, Cheverud JM. The road to modularity. Nature reviews Genetics. 2007; 8:921–931.

Wang HH, Isaacs FJ, Carr PA, Sun ZZ, Xu G, Forest CR, Church GM. Programming cells by multiplex genome engineering and accelerated evolution. Nature. 2009; 460:894–898. [PubMed: 19633652]

Wang J, Atolia E, Hua B, Savir Y, Escalante-Chong R, Springer M. Natural Variation in Preparation for Nutrient Depletion Reveals a Cost–Benefit Tradeoff. PLOS Biology. 2015; 13:e1002041–e1002041. [PubMed: 25626068]

Weinzierl RO. The nucleotide addition cycle of RNA polymerase is controlled by two molecular hinges in the Bridge Helix domain. BMC Biol. 2010; 8:134. [PubMed: 21034443]

Wray GA. The evolutionary significance of cis-regulatory mutations. Nature reviews Genetics. 2007; 8:206–216.

Xia J, Sinelnikov IV, Han B, Wishart DS. MetaboAnalyst 3.0--making metabolomics more meaningful. Nucleic Acids Res. 2015; 43:W251–257. [PubMed: 25897128]

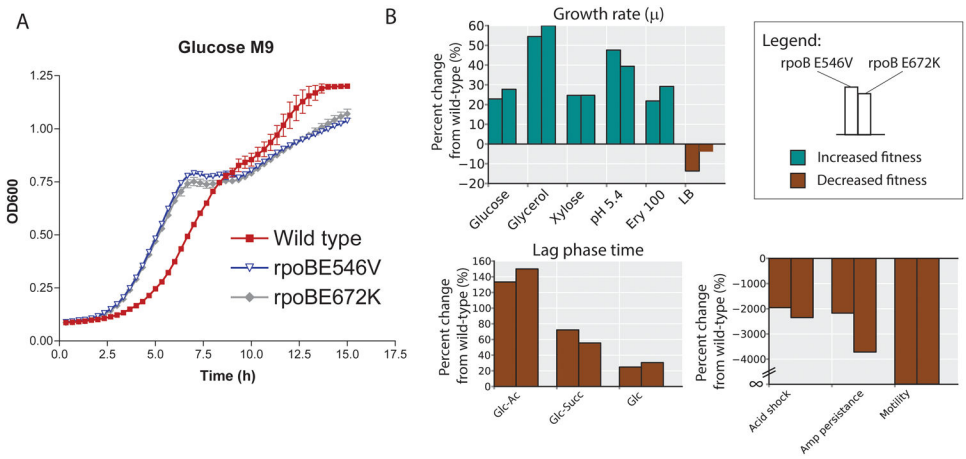

Figure 1. Growth versus hedging antagonistic pleiotropy in organismal phenotypes

A) Adaptive Laboratory Evolution (ALE) -selected *rpoB* mutations (E546V blue, E672K gray) grow faster in the glucose consumption phase but have a longer diauxic shift to grow on acetate than the wild type (red) (Table S1).

B) In addition to growth on glucose (the environment in which the mutants were selected), several additional organismal phenotypes are affected by the *rpoB* mutations. Bar charts show the percent change in measured phenotypes compared to the wild type. Steady-state growth rate increases (cyan) and growth rate in LB medium as well as fitness in environmental shifts and shocks decreases (brown). LB: Luria Broth, Glc: Glucose, Succ: Succinate, Ac: Acetate, Ery 100: 100 μg/mL erythromycin, Amp: Ampicillin.

See also Figure S1 and S2, Table S1 and S2.

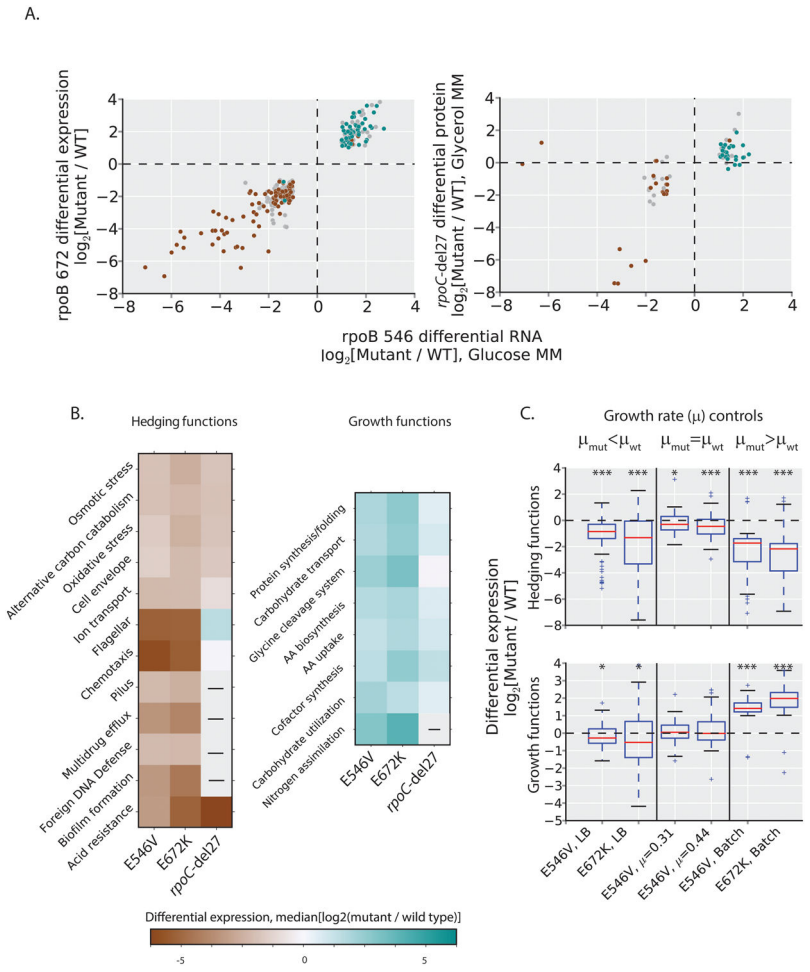

Figure 2. Consistent molecular growth versus hedging response

A) The differential RNA expression in the ALE-selected *rpoB* mutants (E546V, E672K) is consistent (left). The differential RNA expression in glucose is also concordant with the differential protein expression measured in a previous work on glycerol of an ALE-selected 27 aa deletion in β′ compared to the wild type (*rpoC*-del27 (Cheng et al., 2014) right).

B) Functional classification of differentially expressed genes reveals that genes with common functions are often differentially expressed in the same direction, segregating growth (up-regulated, cyan) and hedging (down-regulated, brown) functions. Gray dots are genes with functions that are not consistently differentially expressed. Median differential expression of genes in the functional categories is shown in the heat map; dashes indicate genes not detected in proteomics data (Cheng et al., 2014).

C) Environmental controls disentangle direct effects of the mutations and indirect effects of changes in growth. Box plots show differential expression of identified growth and hedging functions across environments, showing that hedging functions are consistently down-regulated and the expression of growth functions depends on the growth rate. Stars indicate if the mean differential expression of the group of genes is significantly different than zero, based on a two-sided t-test ($p<0.05$, *; $p < 0.0001$, ***).

See also Figure S3 and Table S3.

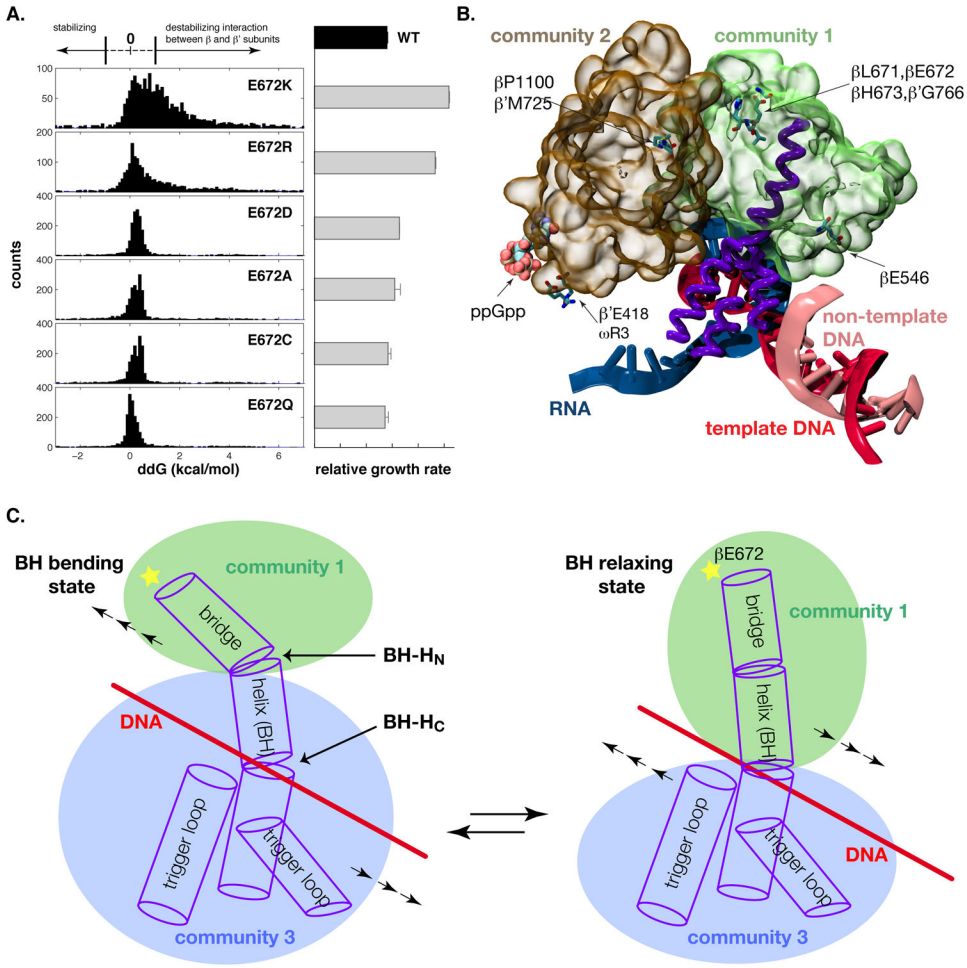

Figure 3. ALE-selected *rpoB* mutations modulate structural dynamic of the *E. coli* RNAP

A) Change in interaction energy between the β & β′ subunits across six different E672 mutations, compared with their corresponding growth rates. To reduce bias from a single static crystal structure, interaction energy is calculated every 25 ps over a 60 ns molecular dynamic trajectory starting from the RNAP open complex.

B) Dynamical community structures encompassing the ALE-selected mutations. Community 1 (green), as discussed in the text, includes the bridge helix in β′ subunit (purple), βE672, βE546, and a few other ALE-selected mutations in contact with βE672. Community 2 (brown) spans the interface between the β & β′ subunits, interacting with community 1 on one side, and the (p)ppGpp binding site on the other.

C) A schematic representation showing how relative movements between the dynamical communities modulates open complex stability. Components are color coded as in panel B. A third community (blue) is identified for calculating the correlated motions with respect to the mutation containing community 1. Continuous arrows show the direction of relative collective motions of the community structures. Effective allosteric communication between distantly located residues can be resolved from optimal path calculated based on a dynamical correlation network. The result shows that βE672 and βE546 share the same optimal dynamical path (orange) towards the (p)ppGpp binding site in the ω subunit. Structural elements are shown from the same perspective, and color-coded the same as in B).

See also Figure S2 and Table S4.

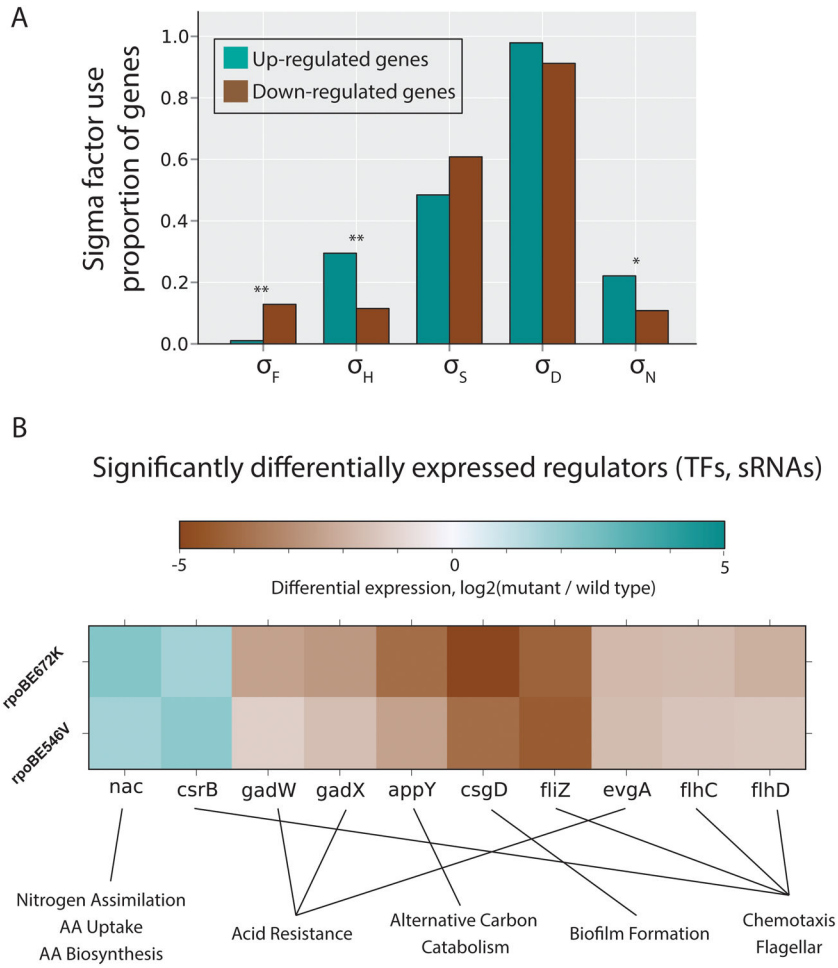

Figure 4. Reprograming of the regulatory network

A) The σ factor usage of differentially expressed genes in mutant strains is shown. Bars indicate the fraction of up-regulated (cyan) and down-regulated (brown) genes that have a promoter that is regulated by a given σ factor. Only σ factors with greater than 10% of promoters regulated among either up-regulated or down-regulated genes are shown. Significant differences in the proportion between σ factor use in up-regulated and down-regulated genes are indicated with asterisks; one asterisk indicates $p<0.05$ and two asterisks indicate $p<0.005$.

B) The fold change for transcription factors and sRNA that are significantly differentially expressed in both mutant strains compared to the wild-type are shown.

See also Figure S4 and Table S3.

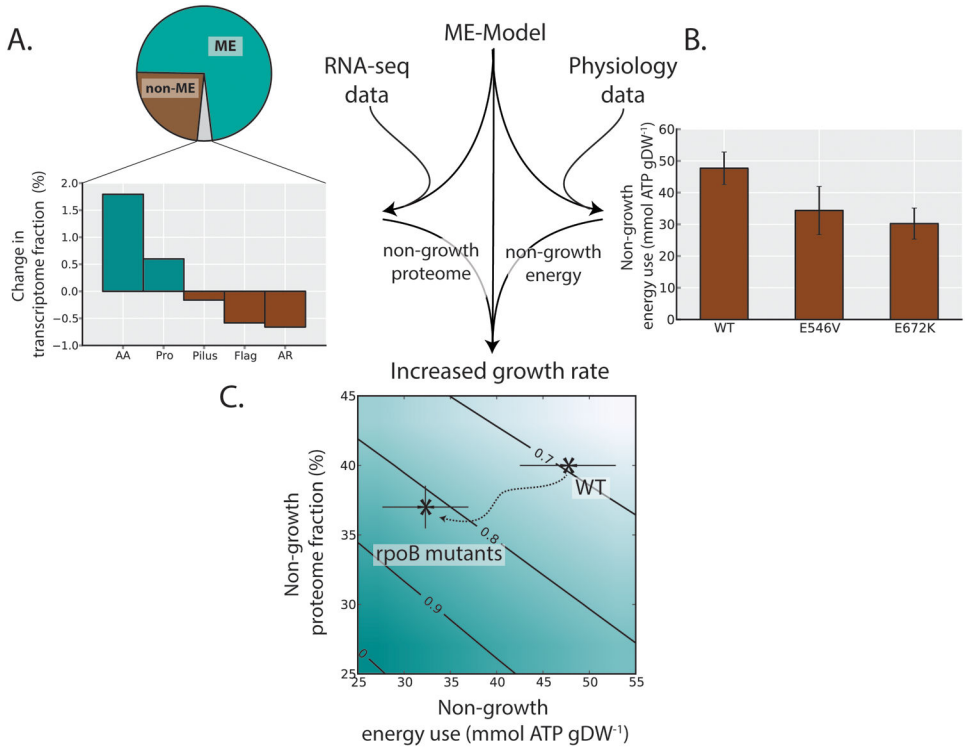

Figure 5. The changes and effects of proteomic and energetic resource allocation

A) A genome-scale model of Metabolism and gene Expression (ME-Model) is used to integrate the RNA-sequencing and physiological data. The transcriptome fraction devoted to ME and non-ME (i.e., not included in the ME-Model) genes is calculated for the wild-type and mutant strains. Grey area of the pie chart indicates the fraction of the transcriptome reallocated from non-ME to ME genes. Bar chart shows the functional categories that reduced or increased in expression by more than 0.1% of the total transcriptome. Abbreviations for the functional categories are: amino acid biosynthesis (AA), protein synthesis/folding (Pro), acid resistance (AR), and flagellar (Fla). All percentages are shown as the average for E546V and E672K.

B) The physiological data was used to calculate the energy use not accounted for by the ME-Model (see Methods, Computation of maximum unaccounted for energy), showing a reduction in unaccounted for energy use in *rpoB* mutants compared to the wild-type. Error bars indicate standard error across biological replicates.

C) The effects of non-ME protein and energy use on maximal growth rates in the ME-Model are computed and shown in the contour plot (see Methods). The wild-type and mutant strains are indicated on the plot, showing how lower non-ME protein and energy use can cause increased growth.

See also Figure S5.

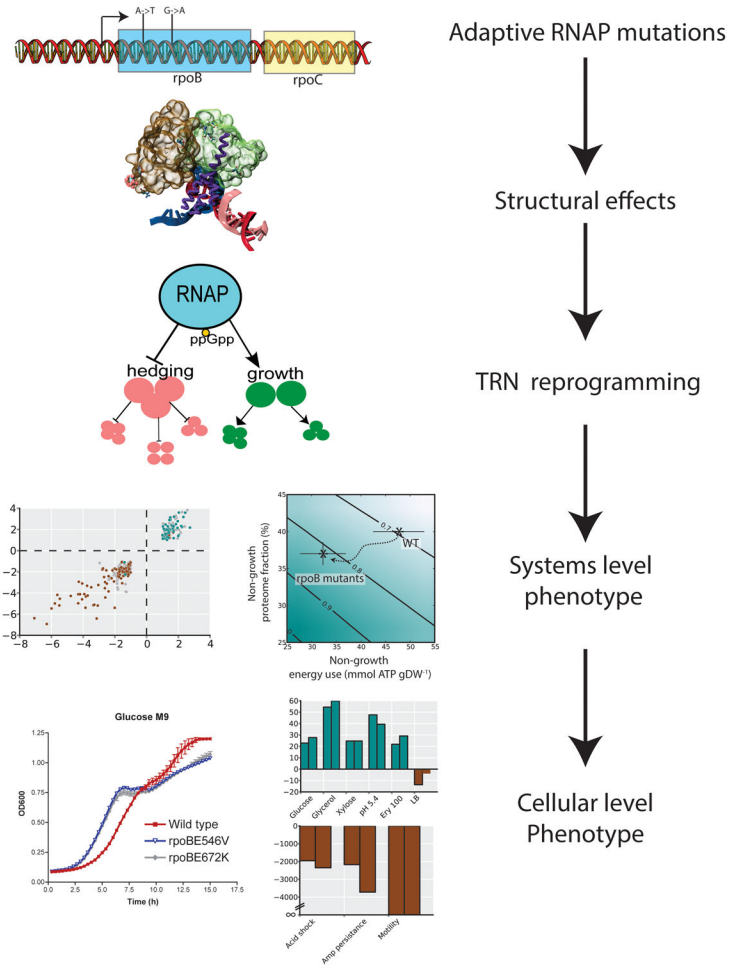

Figure 6. Multi-scale characterization from genotype to phenotype

The multi-scale effects of the studied adaptive regulatory mutations in RNAP are summarized. The mutations alter the structural dynamics of the RNAP, perturbing the transcriptional regulatory network through the action of key transcription factors. The decrease in expression of hedging functions lowers the proteome and energy allocation towards hedging functions and increases cellular growth. In turn, the cell can grow faster in conditions of steady-state growth, but is less fit under environmental shifts and shocks.